Fermilab

First search for atmospheric millicharged particles with the LUX-ZEPLIN experiment

First search for atmospheric millicharged particles with the LUX-ZEPLIN experiment

J. Aalbers,[1,2] D.S. Akerib,[1,2] A.K. Al Musalhi,[3] F. Alder,[3] C.S. Amarasinghe,[4] A. Ames,[1,2] T.J. Anderson,[1,2]
N. Angelides,[5] H.M. Araújo,[5] J.E. Armstrong,[6] M. Arthurs,[1,2] A. Baker,[7] S. Balashov,[8] J. Bang,[9]
J.W. Bargemann,[4] E.E. Barillier,[10,11] D. Bauer,[5] K. Beattie,[12] T. Benson,[13] A. Bhatti,[6] A. Biekert,[12,14]
T.P. Biesiadzinski,[1,2] H.J. Birch,[10,11] E. Bishop,[15] G.M. Blockinger,[16] B. Boxer,[17] C.A.J. Brew,[8] P. Brás,[18]
S. Burdin,[19] M. Buuck,[1,2] M.C. Carmona-Benitez,[20] M. Carter,[19] A. Chawla,[21] H. Chen,[12] J.J. Cherwinka,[13]
Y.T. Chin,[20] N.I. Chott,[22] M.V. Converse,[23] R. Coronel,[1,2] A. Cottle,[3] G. Cox,[24] D. Curran,[24] C.E. Dahl,[25,26]
I. Darlington,[3] S. Dave,[3] A. David,[3] J. Delgaudio,[24] S. Dey,[27] L. de Viveiros,[20] L. Di Felice,[5] C. Ding,[9]
J.E.Y. Dobson,[7] E. Druszkiewicz,[23] S. Dubey,[9] S.R. Eriksen,[28] A. Fan,[1,2] S. Fayer,[5] N.M. Fearon,[27]
N. Fieldhouse,[27] S. Fiorucci,[12] H. Flaecher,[28] E.D. Fraser,[19] T.M.A. Fruth,[29] R.J. Gaitskell,[9] A. Geffre,[24]
J. Genovesi,[20,22] C. Ghag,[3] A. Ghosh,[16] R. Gibbons,[12,14] S. Gokhale,[30] J. Green,[27] M.G.D.van der Grinten,[8]
J.J. Haiston,[22] C.R. Hall,[6] T.J. Hall,[19] S. Han,[1,2] E. Hartigan-O'Connor,[9] S.J. Haselschwardt,[10]
M.A. Hernandez,[10,11] S.A. Hertel,[31] G. Heuermann,[10] G.J. Homenides,[32] M. Horn,[24] D.Q. Huang,[33,*] D. Hunt,[27]
E. Jacquet,[5] R.S. James,[3,†] J. Johnson,[17] A.C. Kaboth,[21] A.C. Kamaha,[33] Meghna K.K.,[16] D. Khaitan,[23]
A. Khazov,[8] I. Khurana,[3] J. Kim,[4] Y.D. Kim,[34] J. Kingston,[17] R. Kirk,[9] D. Kodroff,[12] L. Korley,[10]
E.V. Korolkova,[35] H. Kraus,[27] S. Kravitz,[36] L. Kreczko,[28] V.A. Kudryavtsev,[35] C. Lawes,[7] D.S. Leonard,[34]
K.T. Lesko,[12] C. Levy,[16] J. Lin,[12,14] A. Lindote,[18] W.H. Lippincott,[4] M.I. Lopes,[18] W. Lorenzon,[10] C. Lu,[9]
S. Luitz,[1,37] P.A. Majewski,[8] A. Manalaysay,[12] R.L. Mannino,[38] C. Maupin,[24] M.E. McCarthy,[23] G. McDowell,[10]
D.N. McKinsey,[12,14] J. McLaughlin,[25] J.B. McLaughlin,[3] R. McMonigle,[16] E. Mizrachi,[6,38] A. Monte,[4]
M.E. Monzani,[1,2,39] J.D. Morales Mendoza,[1,2] E. Morrison,[22] B.J. Mount,[40] M. Murdy,[31] A.St.J. Murphy,[15]
A. Naylor,[35] H.N. Nelson,[4] F. Neves,[18] A. Nguyen,[15] C.L. O'Brien,[36] I. Olcina,[12,14] K.C. Oliver-Mallory,[5]
J. Orpwood,[35] K.Y Oyulmaz,[15] K.J. Palladino,[27] J. Palmer,[21] N.J. Pannifer,[28] N. Parveen,[16] S.J. Patton,[12]
B. Penning,[10,11] G. Pereira,[18] E. Perry,[3] T. Pershing,[38] A. Piepke,[32] Y. Qie,[23] J. Reichenbacher,[22] C.A. Rhyne,[9]
A. Richards,[5] Q. Riffard,[12] G.R.C. Rischbieter,[10,11] E. Ritchey,[6] H.S. Riyat,[15] R. Rosero,[30] T. Rushton,[35]
D. Rynders,[24] D. Santone,[21] A.B.M.R. Sazzad,[32] R.W. Schnee,[22] G. Sehr,[36] B. Shafer,[6] S. Shaw,[15] T. Shutt,[1,2]
J.J. Silk,[6] C. Silva,[18] G. Sinev,[22] J. Siniscalco,[3] R. Smith,[12,14] V.N. Solovov,[18] P. Sorensen,[12] J. Soria,[12,14]
I. Stancu,[32] A. Stevens,[3,5] K. Stifter,[26] B. Suerfu,[12,14] T.J. Sumner,[5] M. Szydagis,[16] D.R. Tiedt,[24] M. Timalsina,[12]
Z. Tong,[5] D.R. Tovey,[35] J. Tranter,[35] M. Trask,[4] M. Tripathi,[17] A. Usón,[15] A. Vacheret,[5] A.C. Vaitkus,[9]
O. Valentino,[5] V. Velan,[12] A. Wang,[1,2] J.J. Wang,[32] Y. Wang,[12,14] J.R. Watson,[12,14] L. Weeldreyer,[32]
T.J. Whitis,[4] K. Wild,[20] M. Williams,[10] W.J. Wisniewski,[1] L. Wolf,[21] F.L.H. Wolfs,[23] S. Woodford,[19]
D. Woodward,[12,20] C.J. Wright,[28] Q. Xia,[12] J. Xu,[38] Y. Xu,[33,‡] M. Yeh,[30] D. Yeum,[6] W. Zha,[20] and E.A. Zweig[33]

(The LZ Collaboration)

[1] *SLAC National Accelerator Laboratory, Menlo Park, CA 94025-7015, USA*
[2] *Kavli Institute for Particle Astrophysics and Cosmology,*
Stanford University, Stanford, CA 94305-4085, USA
[3] *University College London (UCL), Department of Physics and Astronomy, London WC1E 6BT, UK*
[4] *University of California, Santa Barbara, Department of Physics, Santa Barbara, CA 93106-9530, USA*
[5] *Imperial College London, Physics Department, Blackett Laboratory, London SW7 2AZ, UK*
[6] *University of Maryland, Department of Physics, College Park, MD 20742-4111, USA*
[7] *King's College London, Department of Physics, London WC2R 2LS, UK*
[8] *STFC Rutherford Appleton Laboratory (RAL), Didcot, OX11 0QX, UK*
[9] *Brown University, Department of Physics, Providence, RI 02912-9037, USA*
[10] *University of Michigan, Randall Laboratory of Physics, Ann Arbor, MI 48109-1040, USA*
[11] *University of Zürich, Department of Physics, 8057 Zürich, Switzerland*
[12] *Lawrence Berkeley National Laboratory (LBNL), Berkeley, CA 94720-8099, USA*
[13] *University of Wisconsin-Madison, Department of Physics, Madison, WI 53706-1390, USA*
[14] *University of California, Berkeley, Department of Physics, Berkeley, CA 94720-7300, USA*
[15] *University of Edinburgh, SUPA, School of Physics and Astronomy, Edinburgh EH9 3FD, UK*
[16] *University at Albany (SUNY), Department of Physics, Albany, NY 12222-0100, USA*
[17] *University of California, Davis, Department of Physics, Davis, CA 95616-5270, USA*
[18] *Laboratório de Instrumentação e Física Experimental de Partículas (LIP),*
University of Coimbra, P-3004 516 Coimbra, Portugal
[19] *University of Liverpool, Department of Physics, Liverpool L69 7ZE, UK*
[20] *Pennsylvania State University, Department of Physics, University Park, PA 16802-6300, USA*
[21] *Royal Holloway, University of London, Department of Physics, Egham, TW20 0EX, UK*
[22] *South Dakota School of Mines and Technology, Rapid City, SD 57701-3901, USA*

[23] University of Rochester, Department of Physics and Astronomy, Rochester, NY 14627-0171, USA
[24] South Dakota Science and Technology Authority (SDSTA),
Sanford Underground Research Facility, Lead, SD 57754-1700, USA
[25] Northwestern University, Department of Physics & Astronomy, Evanston, IL 60208-3112, USA
[26] Fermi National Accelerator Laboratory (FNAL), Batavia, IL 60510-5011, USA
[27] University of Oxford, Department of Physics, Oxford OX1 3RH, UK
[28] University of Bristol, H.H. Wills Physics Laboratory, Bristol, BS8 1TL, UK
[29] The University of Sydney, School of Physics, Physics Road, Camperdown, Sydney, NSW 2006, Australia
[30] Brookhaven National Laboratory (BNL), Upton, NY 11973-5000, USA
[31] University of Massachusetts, Department of Physics, Amherst, MA 01003-9337, USA
[32] University of Alabama, Department of Physics & Astronomy, Tuscaloosa, AL 34587-0324, USA
[33] University of California, Los Angeles, Department of Physics & Astronomy, Los Angeles, CA 90095-1547, USA
[34] IBS Center for Underground Physics (CUP), Yuseong-gu, Daejeon, Korea
[35] University of Sheffield, Department of Physics and Astronomy, Sheffield S3 7RH, UK
[36] University of Texas at Austin, Department of Physics, Austin, TX 78712-1192, USA
[37] Kavli Institute for Particle Astrophysics and Cosmology,
Stanford University, Stanford, CA 94305-4085 USA
[38] Lawrence Livermore National Laboratory (LLNL), Livermore, CA 94550-9698, USA
[39] Vatican Observatory, Castel Gandolfo, V-00120, Vatican City State
[40] Black Hills State University, School of Natural Sciences, Spearfish, SD 57799-0002, USA
(Dated: December 11, 2024)

We report on a search for millicharged particles (mCPs) produced in cosmic ray proton atmospheric interactions using data collected during the first science run of the LUX-ZEPLIN experiment. The mCPs produced by two processes—meson decay and proton bremsstrahlung—are considered in this study. This search utilized a novel signature unique to liquid xenon (LXe) time projection chambers (TPCs), allowing sensitivity to mCPs with masses ranging from 10 to 1000 MeV/c^2 and fractional charges between 0.001 and 0.02 of the electron charge (e). With an exposure of 60 live days and a 5.5 tonne fiducial mass, we observed no significant excess over background. This represents the first experimental search for atmospheric mCPs and the first search for mCPs using an underground LXe experiment.

Millicharged particles (mCPs), denoted as χ, are hypothetical particles carrying a small fractional electric charge to that of an electron $Q_\chi = \epsilon e$. The search for mCPs is closely connected to the research of string theory [1], grand unification theories (GUTs) [2, 3], and the principle of charge quantization [4, 5] which is taken as an observation in the standard model (SM) without firm theoretical motivation. In their simplest theoretical form without considering ultraviolet completeness, mCPs can be incorporated into the SM as new particles carrying a small charge under $U(1)_Y$ gauge symmetry. Other possible origins include kinetic mixing between a dark photon field and the SM hypercharge field [6–8], or extensions to the SM involving mass mixing [9–11]. Consequently, experimental searches for mCPs not only serve as a powerful test of various dark sector models and charge quantization but also represent an important frontier in the exploration of physics beyond the SM.

Several studies [12–14] have proposed that mCPs could constitute a small portion of the dark matter (DM) in the universe, building upon the hypothesis that some fraction of DM may exhibit small electromagnetic interactions with photons [15–19]. This interest in mCPs was

notably revitalized following the anomalous findings from the EDGES experiment in 21-cm cosmology [15, 20, 21], with mCPs as a potential explanation [22–26]. Additionally, experimental searches for the electromagnetic interaction of galactic DM in the mass range of a few GeV/c^2 to TeV/c^2 have been conducted to probe their interactions with nuclei [27–29]. However, for non-relativistic mCPs with smaller masses, the energy deposited during scattering with nuclei becomes small, rendering such searches challenging.

For mCPs with mass in the region 10 to 1500 MeV/c^2, the current experimental limits come from accelerator experiments, including ArgoNeuT [30], milliQan [31], SLACmq [32], SuperCDMS [33] and SENSEI [34]. Recent studies suggest that in this mass range, a substantial flux of relativistic mCPs may be produced through atmospheric cosmic ray interactions, generating detectable energy deposits in terrestrial detectors [35–42]. References [35, 38, 43, 44] showed that liquid xenon (LXe) detectors, albeit smaller than neutrino detectors in size, can set competitive constraints on relativistic atmospheric DM particles, including mCPs [41, 44]. The sensitivity of LXe detectors is due to their comparably low energy threshold and background rates [45]. In this letter, we report on the first search for atmospheric mCPs. This analysis used data collected between December 23, 2021, and May 11, 2022, from the LUX-ZEPLIN (LZ) dark matter experiment during Science Run 1 (SR1), with a

———

* dqhuang@physics.ucla.edu
† Also at The University of Melbourne, School of Physics, Melbourne, VIC 3010, Australia
‡ xuyongheng@physics.ucla.edu

total exposure of 0.91 tonne×year [46].

The LZ experiment [47, 48] is located 4850 ft underground in the Davis Cavern at the Sanford Underground Research Facility (SURF) in Lead, South Dakota. LZ has leading sensitivity to Weakly Interacting Massive Particle (WIMP) dark matter models [46, 49]. At the core of the LZ experiment is a dual-phase xenon time projection chamber (TPC), a vertical cylinder approximately 1.5 meters in diameter and height, containing a 7-tonne active mass. The TPC detects energy depositions in LXe, producing two types of signals: vacuum ultraviolet (VUV) scintillation photons (S1) and ionization electrons. The ionization electrons drift under a near-uniform electric field towards the liquid-gas surface, where they are extracted into the gas region and produce an electroluminescence signal (S2). The S1 and S2 signals are detected by two arrays of 3-inch photomultiplier tubes (PMTs), with 253 PMTs positioned at the top and 241 PMTs at the base of the TPC. The horizontal position (x, y) of an event is reconstructed using the S2 light incident on the top PMT array, and the z-position is calculated from the delay time between S1 and S2 signals. Spatial variations in S1 and S2 signals are corrected using radioactive sources, as in [46], yielding position-independent signals, S1c and S2c. The ratio of S2c to S1c signals is critical for differentiating between nuclear recoil (NR) and electron recoil (ER) interactions. Encasing the TPC, a 'skin' of instrumented LXe and a 17-tonne gadolinium-loaded liquid scintillator outer detector (OD) serve as anti-coincidence detectors, providing shielding and background veto capabilities. Additionally, a 238-tonne ultra-pure water tank surrounds the LZ setup, further enhancing protection against ambient radioactive backgrounds.

As mCPs participate in SM QED processes, the interaction between cosmic rays and atoms in the atmosphere can produce a flux of mCPs detectable by terrestrial detectors. In this analysis, we consider mCPs produced in two distinct atmospheric production processes: meson decay (MD) and proton bremsstrahlung (PB). In the MD channel, neutral mesons are produced during cosmic ray hadronic interactions, leading to the generation of mCP-pairs through electromagnetic decays. The mCP flux from atmospheric meson decays can be calculated with a zenith angle dependence using the cascade equation as in Ref. [50]. For this calculation, we employ the HEAVENLYMCP package [38] which estimates the mCP flux at the Earth's surface from the MD channel, incorporating the meson-mCP branching ratio as detailed in Refs. [35, 36, 51]. In the PB channel, a cosmic ray proton collides with atmospheric atoms and is stopped. The initial state proton emits a bremsstrahlung photon, which subsequently radiates a mCP pair [52–55]. The atmospheric mCP flux at the surface from the PB channel is adopted from the calculations presented in Refs. [39, 42]. The mCP flux at the surface produced from both processes is illustrated in the top panel of Fig. 1.
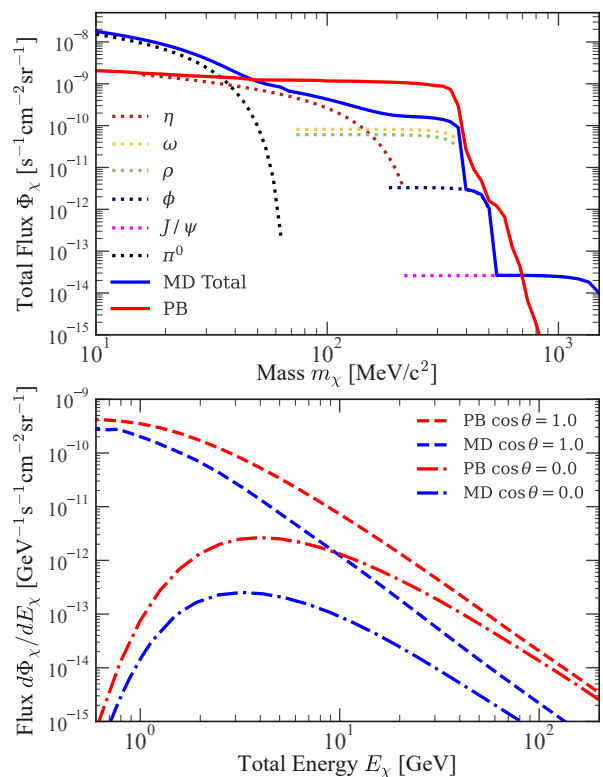
Atmospheric mCPs lose energy through scattering and

FIG. 1. Top panel: the mCP flux integrated over all energies from the PB channel and the MD channel on the surface, as a function of mCP mass m_χ, with $\epsilon = 0.01$ and $\cos\theta = 1.0$. The contributions from each parent meson species to the MD channel are also shown. Bottom panel: the differential mCP energy spectra from the MD and PB channel reaching the LZ detector. As a benchmark, we show the spectra of the mCP model with $m_\chi = 100$ MeV/c^2 and $\epsilon = 0.01$. The underground flux from the vertical direction ($\cos\theta = 1.0$) is represented by the solid lines, and the flux from the horizontal direction ($\cos\theta = 0.0$) is represented by the dot-dashed lines.

ionization as they traverse the overburden on their way to an underground detector. This attenuation effect will reduce the flux reaching the LZ detector, and scales with the charge fraction ϵ and distance traveled through the Earth. To account for this, we employ the energy-loss based attenuation method outlined in Ref. [38] to calculate the attenuated mCP flux reaching the LZ detector, starting from the initial surface flux, with the SURF surface profile as in Ref. [56] taken into consideration. For illustration, the mCP flux produced in both channels reaching the LZ detector from zenith angle $\cos\theta = 1.0$ and 0.0 is shown in the bottom panel of Fig. 1.

To model mCP interactions in the LZ detector, we consider two mCP-xenon interaction models: the free electron model and the photon absorption ionization (PAI) model. We treat the models as separate signals in this analysis. The free electron model [35, 36], which assumes all electrons in LXe are free, is widely used in recent mCP theory searches [35, 38, 39]. The mCP-free electron scat-
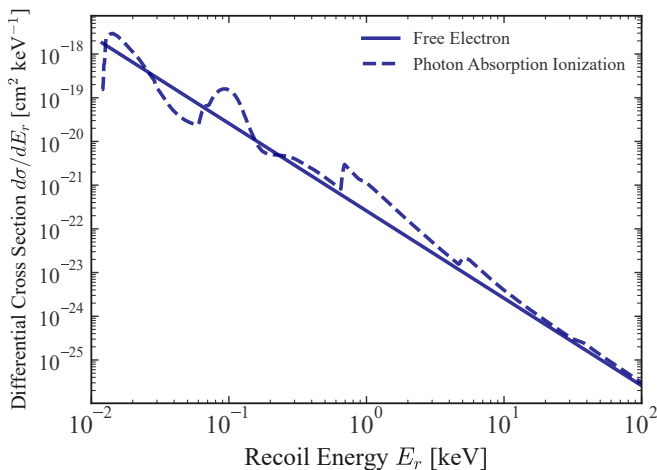
FIG. 2. The differential cross section of mCP-electron interaction in liquid xenon predicted by the free electron model (solid) and the PAI model (dashed). As a benchmark, we take $m_\chi = 100$ MeV/c^2, and $E_\chi = 0.5$ GeV.

tering differential cross section is given by [36]:

$$\frac{d\sigma^{\mathrm{FE}}}{dE_r} = \epsilon^2 \alpha^2 \frac{E_r + 2E_\chi^2/E_r - 2E_\chi - m_e - m_\chi^2/m_e}{E_r m_e (E_\chi^2 - m_\chi^2)}, \quad (1)$$

where α is the fine structure constant, E_r is the recoil energy, m_χ is the mass of the mCP and m_e is the mass of an electron.

The PAI model [57] takes into account the binding energy of electrons using optical constants and has been used in other mCP searches [33, 58]. Following Ref. [59], the optical constants used in the calculation are from Refs. [60] and [61]. The mCP-electron scattering differential cross section predicted by the PAI model is related to that of muons by

$$\frac{d\sigma_\chi^{\mathrm{PAI}}(\beta)}{dE_r} = \epsilon^2 \frac{d\sigma_\mu^{\mathrm{PAI}}(\beta)}{dE_r}, \quad (2)$$

where $\beta = v/c$ is the speed of the ionizing particle, and $\sigma_\mu^{\mathrm{PAI}}$ is the PAI cross section of muons. A comparison of the cross section derived from the two mCP xenon interaction models is shown in Fig. 2. We note that the cross section from both models are approximately inversely proportional to the square of the electron recoil energy E_r. Due to the xenon electron shell structure, the PAI model predicts some peaks near 10, 100 and 1000 eV, which will lead to more scatters near those energies.

To model the detector response to mCPs, we used the LZ simulation framework [56], which incorporates NEST 2.3.12 [62]. The low-energy ER yield model in NEST is constrained by experimental data from [63, 64] and further fine-tuned using *in-situ* tritium calibration data. We simulated mCP tracks through the LZ geometry, using the underground mCP flux shown in Fig. 1 and assuming no deflection in the detector due to their high kinetic energy. Energy deposits along these tracks were

sampled from the mCP-LXe interaction model, and then converted into S1c, S2c, drift time and other observables. Atmospheric mCPs produced in cosmic ray interactions are usually highly relativistic, crossing the LZ TPC in a few nanoseconds. Consequently, S2 pulses, which have a width of microseconds, are unresolvable if the interactions occur at close to the same depth. If the interactions are separated vertically, the individual S2 pulses are resolved due to the relatively slow electron drift. The simulations account for pulse merging by modeling the time separation, pulse widths and pulse areas [56, 65].

For the LZ SR1 operating conditions, an energy deposit of approximately 1 keV is required for both the S1 and S2 pulses to be visible [66]. We found through simulations that mCPs with $\epsilon > 0.001$ undergo multiple scatterings, but that only a small fraction of these scatterings result in a detectable S1-S2 pair. For instance, in the free electron model, a mCP with $m_\chi = 100$ MeV/c^2, $\beta\gamma = 4$, and $\epsilon = 0.005$ has a mean free path of about 30 mm, which is much smaller than the dimensions of the LZ TPC. Nevertheless, most of these scattering events are soft collisions, depositing energies below 1 keV and consequently producing only small S2 pulses, including single-electrons (SE). To produce an above-threshold S1-S2 pair, a scatter needs to deposit an electron recoil energy of around 1 keV or higher. The mean free path for such a hard scatter for the same mCP is approximately 2.2 m, which is comparable to the size of the LZ TPC: about 34% of them crossing the TPC will produce a single hard scatter, and 17% will produce multiple hard scatters. As the charge increases, the proportion of multiple hard scatters will also increase. As a result, a typical mCP crossing the TPC will produce a series of soft scatters (¡ 1 keV) and one or more hard scatters (¿ 1 keV) that result in larger S2 pulses accompanied by visible S1 pulses. This distinct event topology, driven by the differential cross-section of mCP-electron interactions, is characteristic of mCPs and allows LZ to be sensitive to mCPs with charge fractions between 0.001 and 0.02.

To select mCP signals, we search for events featuring a single hard scatter (SHS) that produces a primary S1-S2 pair, along with three or more soft scatters generating small S2s in between. The small S2s after the primary S2 are not considered due to elevated rates of activity after large S2s, as is commonly observed in dual-phase xenon TPCs [67, 68]. The S1 signal must have a threefold PMT coincidence and an S1c of at least 3 phd. The S2 threshold is set at S2c 2000 phd ($\sim$ 1 keV), with S2 signals above this threshold considered primary, and those below considered small S2s. The primary S1 and S2 signals are required to pass the same data quality event selection criteria as in the SR1 WIMP search, except for a prompt OD veto cut and an 'excess area' cut [46]. The prompt OD veto cut removes events with coincident signals in the OD within 300 ns of the TPC signal, and the 'excess area' cut excludes events where the summed area of pulses between S1 and S2 exceeds the S2 pulse area. Both cuts could potentially exclude mCP signals. These criteria

help mitigate backgrounds from accidental coincidences of isolated S1 and S2 pulses while maximizing acceptance of mCP signal events. A region of interest (ROI) is defined in the $\{S1c, \log_{10}(S2c)\}$ observable space. This contour is derived from the simulation of single scatter (SS) events at the 90% confidence level (CL), with energy deposits sampled from the cross-section models. The ROI excludes events arising from unresolved multiple energy deposits in the TPC, as well as nuclear recoils from background neutrons.
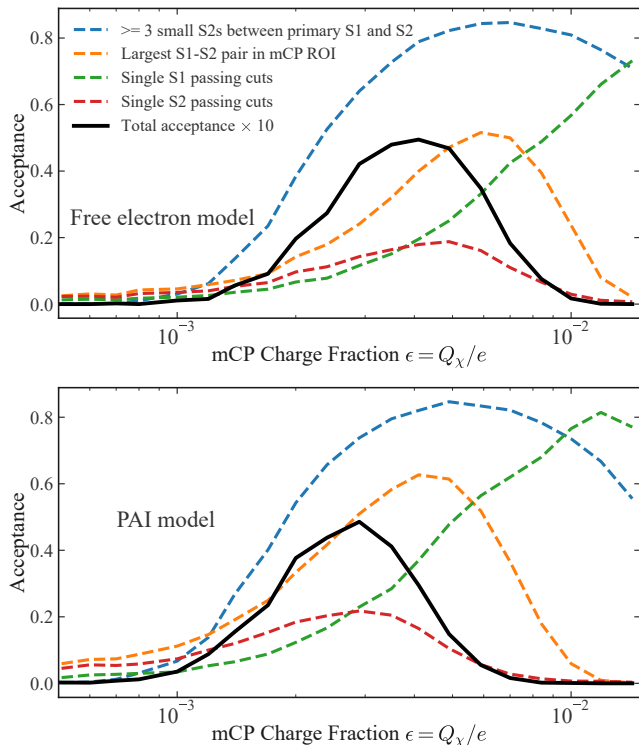
FIG. 3. Acceptances of the data selection cuts evaluated from simulations, defined as number of tracks passing the cut divided by number of tracks simulated. The top panel shows acceptance evaluated using the free electron model, while the bottom panel shows the acceptance evaluated using the PAI model.

The total signal efficiency, shown in Fig. 3, was evaluated from the simulations using the free electron model and PAI model separately. For both interaction models, the efficiency peaks when $\epsilon \simeq 0.003 - 0.004$. For lower charges, the efficiency is mostly suppressed by both the lack of small S2 pulses between primary S1 and S2 and the absence of a hard scatter to create the primary S1-S2 pair. For higher charges, most of the signal loss is from more than one S2 pulses larger than 2000 phd in area, and also the primary S2 merging with other S2s, causing the event to move out of the ROI or fail data quality selection.

Two categories of backgrounds that could potentially mimic mCP signal signatures have been identified. The first consists of SS events that overlap with random small

S2 signals occurring between the primary S1 and S2 signals. The SS background prediction is estimated based on the SR1 WIMP search analysis [45, 46], whose ROI fully encompasses the mCP search ROI (Fig. 4). Prior to applying the requirement of three or more small S2 pulses, a total of 209 ± 22 SS background events are predicted in the mCP ROI. These backgrounds are assessed after the removal of the prompt OD veto and the 'excess area' cuts. To incorporate random small S2 pulses between the primary S1 and S2 signals in the background modeling, we quantify their rate distribution using both sideband data—a time window of the same length as the S1-S2 interval that precedes the S1 (pre-S1 window)—and tritium calibration data. We find that the small S2 rate increases with larger S1 values, primarily due to S1-induced SEs from the photoionization of bulk impurities [67]. Thus, the pre-S1 window, which lacks a preceding S1 signal, provides a lower bound on the small S2 pulse rate distribution. In contrast, the increased activity between the S1 and S2 in the tritium calibration data provides a conservative yet reasonable upper bound for the rate, as tritium events have relatively low energies (≤ 18.6 keV [69]). The pre-S1 window data shows that $(0.07 \pm 0.02)\%$ of events have three or more small S2 pulses between the primary S1 and S2 signals, while tritium data reveals $(0.2 \pm 0.09)\%$ of events exhibit this characteristic. We use [0.07%, 0.2%] as the percentage of events that have three or more small S2 pulses between the S1 and S2. This is validated using a separate sideband dataset of events near the TPC wall, below the NR band mean, under the same conditions as SS background events, ensuring the absence of mCP signals. Out of a total of 698 events, only 1 event exhibited three or more small S2 pulses, which is consistent with the predicted range of [0.5, 1.4] events, calculated by multiplying 698 by [0.07%, 0.2%]. As a further cross-check, the criterion was relaxed to two small S2 pulses, yielding 6 observed events, consistent with the predicted range of [3.5, 6.9].

The second category comprises multiple scatter (MS) background events from detector radioactivity, including gamma rays and neutrons. However, simulations estimate that the expected number of events containing the mCP event topology is ¡ 0.01, rendering this type of background negligible. Combining all the aforementioned factors, the total background expectation is [0.15, 0.42] events, calculated by multiplying the expected number of SS background events (209) by the probability to have an accidental coincidence of three or more small S2 pulses ([0.07%, 0.2%]).

A search for mCPs was performed using LZ SR1 data, applying the same live time cuts as those used in the WIMP search [46]. This resulted in an effective live time of 60 ± 1 days and a fiducial LXe mass of 5.5 ± 0.2 tonnes. After all cuts were applied, no events were observed, which aligns with the expectations from our background model. The probability of observing zero events, given the background prediction, lies between 66% and 86%. The events that pass all selections except the mCP ROI
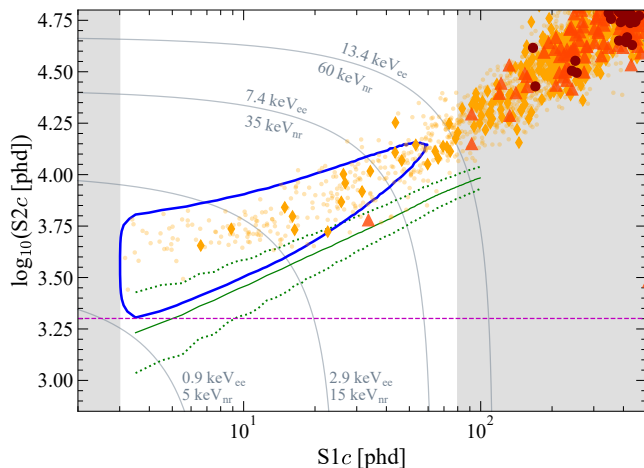
FIG. 4. LZ SR1 mCP search SHS events after data selections, excluding the ROI cut and before applying the three small S2 selection, shown in the $\log_{10}(S2c)$-$S1c$ space within an extended S1 window (up to 500 phd). Events are marked by small orange points (zero small S2 pulses between the primary S1 and S2), orange diamonds (one small S2 pulse), dark-orange triangles (two small S2 pulses), and large filled dark-red circles (three or more small S2 pulses). The trend of increasing small S2 pulses at higher S1 values is due to the increased probability of S1-induced SEs from the photoionization of bulk impurities [67]. The unshaded region denotes the WIMP ROI ($S1c$ 3-80 phd), while solid blue contours show the mCP ROI. The dashed magenta line marks the 2000 phd threshold. The solid green line represents the median of a uniform NR background, with dashed lines indicating the 10% and 90% quantiles. Thin gray lines outline contours of constant energy.

and the three small S2 cuts are depicted in Fig. 4, with the mCP ROI overlaid as a blue contour.

We derive atmospheric mCP exclusion limits following the Feldman-Cousins convention [71] for a 0 observed signal scenario. To derive a conservative constraint, we set the background event expectation at 0.15 events. Atmospheric mCP models that yield more than 2.26 events are excluded at the 90% confidence level. The results are shown in Fig. 5 along with other experimental limits from beam experiments, including ArgoNeuT [30], milliQan demonstrator [31], colliders [70], SLACmq [32] and SEN-SEI [34]. In both mCP-xenon interaction models, after combining contributions from the MD and PB processes, the lower bound of the LZ constraint on atmospheric mCPs is at $\epsilon \sim 0.002$ for mCP masses ¡ 300 MeV/c^2, where the surface mCP flux begins to drop sharply. The excluded region derived from the PAI model is shifted towards lower charges compared to the free electron model, which matches the expectation from the cross sections as shown in Fig. 2. The closed-contour shape of the constraints is from the fact that the selection efficiency drops to zero for $\epsilon < 0.001$ and $\epsilon > 0.01$, as shown in Fig. 3.

In conclusion, we have presented the inaugural experimental search for mCPs produced in cosmic ray atmo-
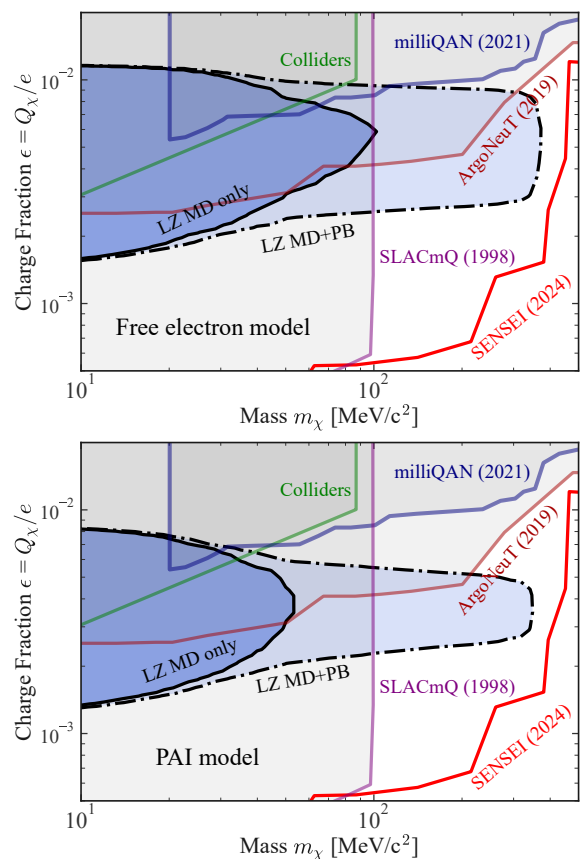
FIG. 5. The 90% CL limits on mCP fractional charge $\epsilon = Q_\chi/e$ derived from atmospheric production channels, as a function of mCP mass m_χ, assuming two mCP-electron interaction models: the free electron model (top) and the PAI model (bottom). The black solid lines are the constraints from the MD process only, and dot-dashed lines are from both the MD and PB processes combined. Selected limits on mCPs from beam experiments are also shown [30–32, 34, 70].

spheric interactions, which is highly complementary to existing results from accelerator-based experiments. We have considered mCPs originating from two production channels: meson decay and proton bremsstrahlung, and conducted the search using a signature novel to liquid xenon detectors. Utilizing data from LZ SR1, we found the data to be consistent with the background-only hypothesis for all tested mCP model parameters, and based on this result, we set new constraints on atmospheric mCP models.

Appendix A: Data Release

Selected data from this letter are available at https://tinyurl.com/LZDataReleaseSR1mCP, including:

- Figure 4: SR1 mCP search data after selection, presented in the format (S1c, $\log_{10}$(S2c), small S2 count between the primary S1 and S2).

- Figure 5: Points representing the 90% CL exclusion contours of MD only and MD+PAI combined, in the free electron and PAI model.

[1] X.-G. Wen and E. Witten, Nuclear Physics B **261**, 651 (1985).
[2] J. C. Pati and A. Salam, Phys. Rev. D **8**, 1240 (1973).
[3] H. Georgi, AIP Conf. Proc. **23**, 575 (1975).
[4] P. A. M. Dirac, Proc. Roy. Soc. Lond. **A133**, 60 (1931), [,278(1931)].
[5] M. I. Dobroliubov and A. Y. Ignatiev, Phys. Rev. Lett. **65**, 679 (1990).
[6] B. Holdom, Phys. Lett. B **166**, 196 (1986).
[7] B. Holdom, Phys. Lett. B **178**, 65 (1986).
[8] R. Foot and X.-G. He, Phys. Lett. B **267**, 509 (1991).
[9] B. Kors and P. Nath, Phys. Lett. B **586**, 366 (2004), arXiv:hep-ph/0402047.
[10] K. Cheung and T.-C. Yuan, JHEP **03**, 120 (2007), arXiv:hep-ph/0701107.
[11] D. Feldman, Z. Liu, and P. Nath, Phys. Rev. D **75**, 115001 (2007), arXiv:hep-ph/0702123.
[12] D. E. Brahm and L. J. Hall, Phys. Rev. D **41**, 1067 (1990).
[13] J. L. Feng, M. Kaplinghat, H. Tu, and H.-B. Yu, JCAP **07**, 004 (2009), arXiv:0905.3039 [hep-ph].
[14] J. M. Cline, Z. Liu, and W. Xue, Phys. Rev. D **85**, 101302 (2012), arXiv:1201.4858 [hep-ph].
[15] R. Barkana, Nature **555**, 71 (2018), arXiv:1803.06698

[astro-ph.CO].

[16] M. Pospelov and T. ter Veldhuis, Phys. Lett. B **480**, 181 (2000), arXiv:hep-ph/0003010.

[17] S. Raby and G. West, Phys. Lett. B **194**, 557 (1987).

[18] K. Sigurdson, M. Doran, A. Kurylov, R. R. Caldwell, and M. Kamionkowski, Phys. Rev. D **70**, 083501 (2004), [Erratum: Phys.Rev.D 73, 089903 (2006)], arXiv:astro-ph/0406355.

[19] O. Antipin, M. Redi, A. Strumia, and E. Vigiani, JHEP **07**, 039 (2015), arXiv:1503.08749 [hep-ph].

[20] A. Boyarsky, D. Iakubovskyi, O. Ruchayskiy, A. Rudakovskyi, and W. Valkenburg, Phys. Rev. D **100**, 123005 (2019), arXiv:1904.03097 [astro-ph.CO].

[21] Q. Li and Z. Liu, Chin. Phys. C **46**, 045102 (2022), arXiv:2110.14996 [hep-ph].

[22] J. B. Muñoz and A. Loeb, Nature **557**, 684 (2018), arXiv:1802.10094 [astro-ph.CO].

[23] A. Berlin, D. Hooper, G. Krnjaic, and S. D. McDermott, Phys. Rev. Lett. **121**, 011102 (2018), arXiv:1803.02804 [hep-ph].

[24] E. D. Kovetz, V. Poulin, V. Gluscevic, K. K. Boddy, R. Barkana, and M. Kamionkowski, Phys. Rev. D **98**, 103529 (2018), arXiv:1807.11482 [astro-ph.CO].

[25] C. Creque-Sarbinowski, L. Ji, E. D. Kovetz, and M. Kamionkowski, Phys. Rev. D **100**, 023528 (2019), arXiv:1903.09154 [astro-ph.CO].

[26] R. Barkana, N. J. Outmezguine, D. Redigolo, and T. Volansky, Phys. Rev. D **98**, 103005 (2018), arXiv:1803.03091 [hep-ph].

[27] X. Ning *et al.* (PandaX), Nature **618**, 47 (2023).

[28] P. Adhikari *et al.* (DEAP), Phys. Rev. D **102**, 082001 (2020), [Erratum: Phys.Rev.D 105, 029901 (2022)], arXiv:2005.14667 [astro-ph.CO].

[29] B. Ali *et al.* (PICO), Phys. Rev. D **106**, 042004 (2022), arXiv:2204.10340 [astro-ph.CO].

[30] R. Acciarri *et al.* (ArgoNeuT), Phys. Rev. Lett. **124**, 131801 (2020), arXiv:1911.07996 [hep-ex].

[31] A. Ball *et al.* (milliQan), Phys. Rev. D **104**, 032002 (2021), arXiv:2104.07151 [hep-ex].

[32] A. A. Prinz *et al.*, Phys. Rev. Lett. **81**, 1175 (1998), arXiv:hep-ex/9804008.

[33] I. Alkhatib *et al.* (SuperCDMS), Phys. Rev. Lett. **127**, 081802 (2021), arXiv:2011.09183 [hep-ex].

[34] L. Barak *et al.* (SENSEI), SENSEI: Search for Millicharged Particles produced in the NuMI Beam (2023), arXiv:2305.04964 [hep-ex].

[35] R. Harnik, R. Plestid, M. Pospelov, and H. Ramani, Phys. Rev. D **103**, 075029 (2021), arXiv:2010.11190 [hep-ph].

[36] R. Plestid, V. Takhistov, Y.-D. Tsai, T. Bringmann, A. Kusenko, and M. Pospelov, Phys. Rev. D **102**, 115032 (2020), arXiv:2002.11732 [hep-ph].

[37] M. Kachelriess and J. Tjemsland, Astropart. Phys. **132**, 102622 (2021), arXiv:2104.06811 [hep-ph].

[38] C. A. Argüelles Delgado, K. J. Kelly, and V. Muñoz Albornoz, JHEP **11**, 099 (2021), arXiv:2104.13924 [hep-ph].

[39] M. Du, R. Fang, and Z. Liu, JHEP **08**, 174 (2024), arXiv:2211.11469 [hep-ph].

[40] M. Du, R. Fang, Z. Liu, W. Lu, and Z. Ye, JHEP **11** (2023), arXiv:2308.05607 [hep-ph].

[41] J. Alvey, M. Campos, M. Fairbairn, and T. You, Phys. Rev. Lett. **123**, 261802 (2019), arXiv:1905.05776 [hep-ph].

[42] H. Wu, E. Hardy, and N. Song, Searching for heavy millicharged particles from the atmosphere (2024), arXiv:2406.01668 [hep-ph].

[43] M. Pokrandt, Master's thesis, KIT, Karlsruhe, IAP (2021).

[44] X. Ning *et al.* (PandaX), Phys. Rev. Lett. **131**, 041001 (2023), arXiv:2301.03010 [hep-ex].

[45] J. Aalbers *et al.* (LZ), Phys. Rev. D **108**, 012010 (2023), arXiv:2211.17120 [hep-ex].

[46] J. Aalbers *et al.* (LZ), Phys. Rev. Lett. **131**, 041002 (2023), arXiv:2207.03764 [hep-ex].

[47] D. S. Akerib *et al.* (LZ), Nucl. Instrum. Meth. A **953**, 163047 (2020), arXiv:1910.09124 [physics.ins-det].

[48] B. J. Mount *et al.*, LUX-ZEPLIN (LZ) Technical Design Report (2017), arXiv:1703.09144 [physics.ins-det].

[49] J. Aalbers *et al.* (LZ Collaboration), Dark Matter Search Results from 4.2 Tonne-Years of Exposure of the LUX-ZEPLIN (LZ) Experiment (2024), arXiv:2410.17036 [hep-ex].

[50] G. Ingelman, Thunman, and P. M. Gondolo, Astropart. Phys. **5**, 309 (1996), arXiv:hep-ph/9505417.

[51] D. Gorbunov, I. Krasnov, Y. Kudenko, and S. Suvorov, Phys. Lett. B **822**, 136641 (2021), arXiv:2103.11814 [hep-ph].

[52] S. N. Gninenko, D. V. Kirpichnikov, and N. V. Krasnikov, Phys. Rev. D **100**, 035003 (2019), arXiv:1810.06856 [hep-ph].

[53] E. Fermi, Z. Phys. **29**, 315 (1924).

[54] E. J. Williams, Phys. Rev. **45**, 729 (1934).

[55] C. F. von Weizsacker, Z. Phys. **88**, 612 (1934).

[56] D. S. Akerib *et al.* (LZ), Astropart. Phys. **125**, 102480 (2021), arXiv:2001.09363 [physics.ins-det].

[57] W. W. M. Allison and J. H. Cobb, Ann. Rev. Nucl. Part. Sci. **30**, 253 (1980).

[58] A. A. Aguilar-Arevalo *et al.* (CONNIE, Atucha-II), (2024), arXiv:2405.16316 [hep-ex].

[59] K. Bihari Prasad, Ph.D. thesis, Texas A-M (2013).

[60] The center for x-ray optics, https://cxro.lbl.gov/, accessed: 2024-07-18.

[61] E. D. Palik and E. J. Prucha, *Handbook of optical constants of solids* (Academic Press, Boston, MA, 1997).

[62] M. Szydagis *et al.*, Noble element simulation technique (2023).

[63] D. S. Akerib *et al.* (LUX), Phys. Rev. D **96**, 112011 (2017), arXiv:1709.00800 [physics.ins-det].

[64] E. M. Boulton *et al.*, JINST **12** (08), P08004, arXiv:1705.08958 [physics.ins-det].

[65] J. Allison *et al.*, Nucl. Instrum. Meth. A **835**, 186 (2016).

[66] J. Aalbers *et al.* (LZ), Phys. Rev. D **108**, 072006 (2023), arXiv:2307.15753 [hep-ex].

[67] D. S. Akerib *et al.* (LUX), Phys. Rev. D **102**, 092004 (2020), arXiv:2004.07791 [physics.ins-det].

[68] P. Sorensen, Electron train backgrounds in liquid xenon dark matter search detectors are indeed due to thermalization and trapping (2017), arXiv:1702.04805 [physics.ins-det].

[69] D. S. Akerib *et al.* (LUX), Phys. Rev. D **93**, 072009 (2016), arXiv:1512.03133 [physics.ins-det].

[70] S. Davidson, S. Hannestad, and G. Raffelt, JHEP **05**, 003 (2000), arXiv:hep-ph/0001179.

[71] G. J. Feldman and R. D. Cousins, Phys. Rev. D **57**, 3873 (1998), arXiv:physics/9711021.

[72] P. Faulkner *et al.*, J. Phys. G **32**, N1 (2005).

[73] D. Britton *et al.*, Philos. Trans. R. Soc. A **367**, 2447 (2009).